Pergamon

Int. J. Heat Mass Transfer. Vol. 40, No. 9, pp. 2035–2043, 1997

0017–9310/97 $17.00+0.00

PII: S0017–9310(96)00283–9

Gas segregation during solidification processes

MARCUS V. A. BIANCHI and RAYMOND VISKANTA†

Heat Transfer Laboratory, School of Mechanical Engineering, Purdue University, West Lafayette, IN 47907-1288, U.S.A.

(*Received* 29 *January* 1996 *and in final form* 8 *August* 1996)

Abstract—Gas pores appear during solidification when the gas concentration in the liquid is higher than the gas solubility at a certain location. In this study, an analysis has been carried out to predict the gas concentration in the melt for different forms of the solidification rate. An exact solution is found for a constant interface velocity. An integral analysis is used to predict the gas concentration behavior for different interface velocity functions, including the most common cases of casting. The maximum gas concentration occurs at the solid–liquid interface and it depends on the form of the solidification rate as a function of time. The results can be used to establish criteria for the maximum amount of dissolved gas permissible in the melt in order to avoid the formation of gas bubbles. © 1997 Elsevier Science Ltd. All rights reserved.

1. INTRODUCTION

Solidification is an important phenomenon occurring in a variety of processes in diverse fields ranging from metals casting to preservation of biological materials. In metallurgy, solidification is often the beginning of any metal production and occurs in such processes as die casting and continuous casting, welding, soldering and metal coating. In particular, casting is a very economic method of forming a component if the melting point of the metal is not too high. It is possible to cast metal products economically from alloys of melting points as high as 1933 K (Ti) [1].

Gas voids and porosity are caused by the evolution and entrapment of gas during the solidification of metals. This gas may result from several sources: (i) a decrease in solubility upon cooling from the liquid state; (ii) reaction of metallic oxides with carbon to form CO and CO_2; and (iii) the reaction of liquid metal with moisture in green sand molds [2]. The primary effects of gas holes and porosity are that they reduce the load carrying capability of the member in which they occur and act as stress concentrators [2].

Although pressure drop due to shrinkage may create a condition for bubble nucleation, for a pure substance the most important mechanism of gas pore formation is the difference in gas solubility between the solid and the liquid. The solubility of a gas in the solid can be orders of magnitude smaller than that in the liquid. The interface rejects gas to the liquid, increasing the concentration of the gas close to the interface and, when the gas concentration is the liquid reaches the gas solubility, nucleation of gas bubbles can occur.

The study of the effects of gases on the solidification of metals began over 150 years ago, but the subject started to receive more attention in the early 1900s [3]. Keeping combustion gases away from the melt and allowing the metal to freeze in the pot, then remelting it as fast as possible, were adopted as solutions to minimize porosity in aluminum. Even so, the rejections were high and "gas in aluminum" was even then recognized as a problem [3].

Wilcox and Kuo [4] theoretically studied the gas bubble nucleation during the crystallization of a multicomponent gas solution. They found that the tendency to form gas bubbles increases with increasing growth rate, decreasing stirring, increasing ambient gas pressure, and decreasing height of liquid over crystal. It was also observed that, although homogeneous nucleation of bubbles is possible, it is most likely that heterogeneous nucleation on the crystal surface is the main mechanism for bubble formation.

The development of blowholes during the solidification of solutions of carbon dioxide in water were experimentally studied by Vasconcellos and Beech [5]. A test cell was designed and the experiments were conducted under different pressure conditions. It was concluded that the form of blowholes associated with the planar ice/water interface may be explained in terms of the solute profile, even though the authors used a steady-state solution of the solute redistribution.

Nucleation and evolution of gas bubbles ahead of a solidification front were theoretically and experimentally studied for magnetoelectric composite materials contaminated with a volatile component (P in Si, for instance) [6]. The author concluded that there are three ways to prevent the formation of gas bubbles ahead of a solidification front in a liquid

† Author to whom correspondence should be addressed.

NOMENCLATURE

a	coefficients of the polynomial representation of C^*
C	gas concentration
C^*	dimensionless gas concentration, $(C-C_i)/(C_S-C_i)$
c_p	specific heat at constant pressure
D	binary diffusion coefficient of the gas in the liquid
H_f	latent heat of fusion
I	dimensionless integral of the velocity ratio, $\int_0^\tau \xi(\sigma)\,d\sigma$
j	number of the term of the polynomial representation of C^*
n	number of terms of the polynomial representation of C^*
S	gas solubility in the liquid phase
T_0	initial sand mold temperature, equation (11)
T_M	melting temperature, equation (11)
t	time
V	solidification rate (solid–liquid interface velocity)
x	coordinate measured from the solid–liquid interface, see Fig. 1
Y	transformed dimensionless gas concentration, equation (19).

Greek symbols

α	thermal diffusivity
β	constant, equation (11)
γ	integral of the dimensionless gas concentration from 0 to δ, $\int_0^\delta C^*\,d\chi$
δ	dimensionless thickness of the diffusion layer
δ_d	thickness of the diffusion layer (length dimension)
ε	dimensionless number, δ^2/τ
η	coefficient of the terms a_i, equation (28)
ξ	dimensionless interface velocity, $V(t)/V_r$
σ	dummy integration variable
χ	dimensionless space variable, $V_r x/D$
τ	dimensionless time, $V_r^2 t/D$.

Subscripts

i	refers to initial condition
j	number of the term of the polynomial representation of C^*
L	refers to the liquid phase
m	refers to the mold
r	reference
S	refers to the solid phase.

contaminated with a volatile: avoiding high contamination, setting low interface velocities (i.e. low solidification rates), and setting extremely high solidification rates.

Void formation in unidirectional solidification of cyclohexane was experimentally studied for both gassed and degassed liquid [7]. Blowholes were observed when gassed liquids were solidified from above and from below. Sulfredge *et al.* [8] performed experiments to understand the void formation during the solidification of cyclohexane and 1,4-butanediol, $C_4H_{10}O_2$. The liquid was degassed before solidification through the use of vacuum and proved to be an important factor in the experiments performed.

Although the phenomenon of gas porosity formation has received considerable research attention, there is a need for additional work that leads to quantification of the gas segregation due to the moving solid–liquid front. The present work introduces and solves the gas species concentration equation for any interface velocity as a function of time. An analytical solution of the model equations is obtained for a constant solidification rate, and an integral method is employed to solve for any solidification rate function. Discussion of the solution for the cases of constant interface velocity and of interface inversely proportional to the square root of time are presented, and qualitative experimental validation is shown.

2. MODEL EQUATIONS

Consider a planar solidification front which is initially stationary. Figure 1 shows the schematic diagram of the model and the coordinate system. The concentration of gas dissolved in the melt is C_i. Suddenly, motion of the interface at velocity $V(t)$ is imposed due to the solidification process. The gas concentration in the liquid $C(x, t)$, when buoyancy effects are negligible, is described by the equation

$$\frac{\partial C}{\partial t} - V(t)\frac{\partial C}{\partial x} = D\frac{\partial^2 C}{\partial x^2}, \tag{1}$$

where D is the binary diffusion coefficient of the gas in the liquid, which is assumed constant and independent of the temperature.

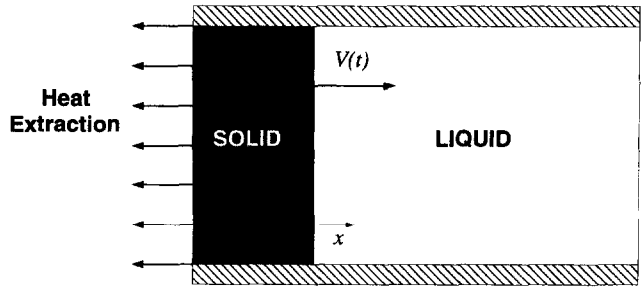

Fig. 1. Schematic diagram for plane front solidification.

Before any solid is formed, the concentration of the gas dissolved in the liquid is uniform:

$$C(x,0) = C_i \quad \text{at } t = 0. \tag{2}$$

At the solid–liquid interface the gas concentration is conserved. The concentration of gas in the solid is assumed constant and equal to C_S. The boundary condition can be expressed as

$$V[C(0,t) - C_S] = -D\frac{\partial C}{\partial x}(0,t) \quad \text{at } x = 0. \tag{3}$$

The remaining boundary condition is given by

$$C(\infty,0) \to C_i \quad \text{at } x \to \infty. \tag{4}$$

Introducing the dimensionless variables χ, τ and C^*, the species conservation equation (1) becomes

$$\frac{\partial C^*}{\partial \tau} - \xi(\tau)\frac{\partial C^*}{\partial \chi} = \frac{\partial^2 C^*}{\partial \chi^2}. \tag{5}$$

The initial and the boundary conditions become, respectively,

$$C^*(\chi,0) = 0 \quad \text{at } \tau = 0, \tag{6}$$

$$\xi(\tau)[C^*(0,\tau) - 1] = -\frac{\partial C^*}{\partial \chi}(0,\tau) \quad \text{at } \chi = 0, \tag{7}$$

$$C^*(\infty,0) \to 0 \quad \text{at } \chi \to \infty. \tag{8}$$

Equations (5)–(8) define the gas species diffusion in the liquid, but the dimensionless solidification rate, $\xi(\tau)$, needs to be chosen in order to completely define the problem. The interface velocity $V(t)$ is a consequence of the solidification process and it creates the driving force for the gas diffusion due to the rejection of gas species from the solid to the liquid phase. Two different solidification rate functions have been studied because of their importance in real systems: constant solidification rate, and solidification rate inversely proportional to the square root of the time. However, the integral solution presented in Section 5 of this paper can be used with any interface velocity function.

Some manufacturing processes impose a constant velocity to the solid–liquid interface, such as unidirectional solidification and Czochralski crystal growth [9]. For this case,

$$V(t) = V_r \quad \text{and} \quad \xi(\tau) = 1. \tag{9}$$

Another very important case is that of a solidification rate inversely proportional to $t^{1/2}$, because it occurs in several different solidification processes, such as during the solidification in sand molds and solidification in metal molds (for both constant casting surface temperature and when there are gradients within mold and casting with or without interface resistance) [9]. The dimensionless velocity function is

$$\xi(\tau) = \frac{1}{\sqrt{\tau}}. \tag{10}$$

The reference velocity V_r is defined depending on the process. Two examples are

$$V_r = \frac{(T_M - T_0)\sqrt{k_m \rho_m c_{pm}}}{\rho_L D H_f \sqrt{\pi}} \quad \text{(sand molds)}$$

$$\text{and} \quad V_r = \frac{\beta\sqrt{\alpha_m}}{D} \quad \text{(metal molds)}, \tag{11}$$

where β is the root of a transcendental equation, depending on the type of mold considered [9].

3. SCALE ANALYSIS

A scale analysis is used in order to obtain order-of-magnitude estimates of the maximum gas concentration, which is located at the solid–liquid interface. This is important because with a minimum effort it is possible to find the functional dependence of the gas concentration at the interface. Details on how to perform a scale analysis can be found elsewhere [10]. The analysis starts by examining the order of magnitude of the three terms present in the gas species conservation equation (1). The terms scale as

$$\underbrace{\frac{\partial C}{\partial t} \sim \frac{\Delta C}{t}}_{\text{Storage}}, \quad \underbrace{V(t)\frac{\partial C}{\partial x} \sim V(t)\frac{\Delta C}{\delta_d}}_{\text{Advection}}$$

$$\text{and} \quad \underbrace{D\frac{\partial^2 C}{\partial x^2} \sim D\frac{\Delta C}{\delta_d^2}}_{\text{Diffusion}}, \tag{12}$$

where $\Delta C = C(x = 0, t) - C_i$ is the scale of the gas concentration. To investigate the order of magnitude

of the maximum gas concentration, the integral form of equation (1) is used

$$\frac{\partial}{\partial \tau}\int_0^{\delta} C^* \, d\chi = -\xi. \tag{13}$$

Evaluating the order of magnitude of the terms of equation (13) one can show that

$$C^*(0,\tau) \sim -\frac{\xi\tau}{\delta}. \tag{14}$$

This result is used in conjunction with the two possible limiting cases. Advection is the driving force and it is, therefore, never negligible. The question to be answered is which of the two terms (storage or diffusion or both) plays the dominant role, or are all three terms of the same order of magnitude. The relative importance of advection and storage can be examined through the ratio $\varepsilon = \delta_d^2/Dt = \delta^2/\tau$. When $\varepsilon \ll 1$, gas species storage is negligible and diffusion must balance advection. On the other hand, when $\varepsilon \gg 1$, gas diffusion is negligible and storage balances advection. The value of ε depends on the value of δ, which is regulated by the value of $\xi(\tau)$. Therefore, the form of the interface velocity dictates the relative importance of the terms at different times.

When gas advection is of the same order of magnitude as gas diffusion, the scaling analysis predicts that

$$\delta \sim \frac{1}{\xi(\tau)}. \tag{15}$$

The interface gas concentration scales as

$$C^*(0,\tau) \sim -\xi^2\tau. \tag{16}$$

For the limiting case when gas diffusion is negligible (advection balances storage), one can show that

$$\delta \sim \tau\xi(\tau). \tag{17}$$

The interface gas concentration scales as

$$C^*(0,\tau) \sim -1. \tag{18}$$

4. ANALYTICAL SOLUTION AND RESULTS

For the particular case where the solidification rate is constant and equal to V_r, it is possible to solve equation (5) analytically. First, the advection term in equation (5) is eliminated through the following transformation:

$$Y(\chi,\tau) = e^{\chi/2+\tau/4} C^*(\chi,\tau). \tag{19}$$

Then, using the Laplace transform technique, the transformed equation and boundary conditions, the problem can be inverted to yield the solution,

$$C^*(\chi,\tau) = 2\sqrt{\frac{\tau}{\pi}} e^{-(\chi^2/4\tau)-(\chi/2)-(\tau/4)} + (1-\chi+\tau)e^{-\chi} \times \operatorname{erfc}\left(\frac{\chi}{2\sqrt{\tau}} + \frac{\sqrt{\tau}}{2}\right) - e^{-\chi}\operatorname{erfc}\left(\frac{\chi}{2\sqrt{\tau}} - \frac{\sqrt{\tau}}{2}\right). \tag{20}$$

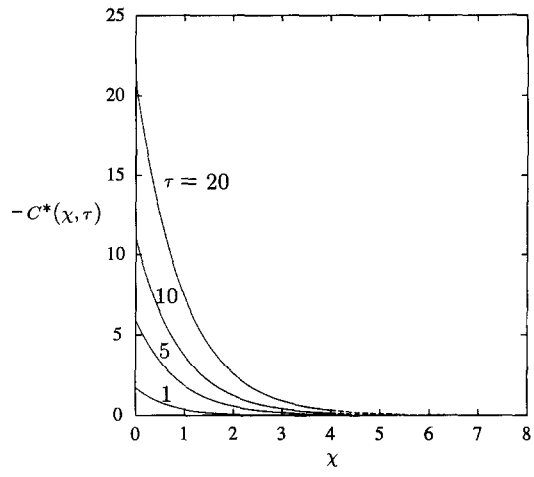

Fig. 2. Concentration profiles for constant interface velocity ($\xi = 1$).

Concentration profiles obtained from equation (20) for τ of 1, 5, 10 and 20 are shown in Fig. 2. As expected, the interface concentration increases rather rapidly with time. Note that the diffusion boundary layer thickness δ increases for early times but stays rather constant for values of τ greater than 5.

The results presented in Fig. 2 can be explained by examining the predictions of the scale analysis. For small values of τ storage balances advection and one can show that $\delta \sim \tau\xi(\tau) = \tau$. Hence, the gas diffusion boundary layer growth is directly proportional to the dimensionless time τ for small values of τ. On the other hand, when $\tau \gg 1$ gas diffusion dominates and storage is negligible ($\varepsilon \ll 1$), and $\delta \sim 1/\xi(\tau) = 1$. Therefore, when $\tau \gg 1$, the gas diffusion boundary layer thickness is rather constant, and this is evident from Fig. 2.

The gas concentration is maximum at the solid–liquid interface ($\chi = 0$) and this is the location where nucleation is most likely to occur. The gas concentration $-C^*(0,\tau)$ is shown in Fig. 3. For small values of τ the interface gas concentration increases very rapidly, but for later times τ the function becomes a straight line with the following equation

$$C^*(0,\tau) = -(1+\tau), \quad \text{for } \tau \gg 1. \tag{21}$$

The result is expected from the scale analysis. At early times gas species storage balances advection, and equation (18) states that $C^*(0,\tau) \sim -1$. On the other hand, for $\tau \gg \delta$ ($\varepsilon \gg 1$) the result given by equation (16) is valid, $C^*(0,\tau) \sim -\xi^2\tau = -\tau$. This result is

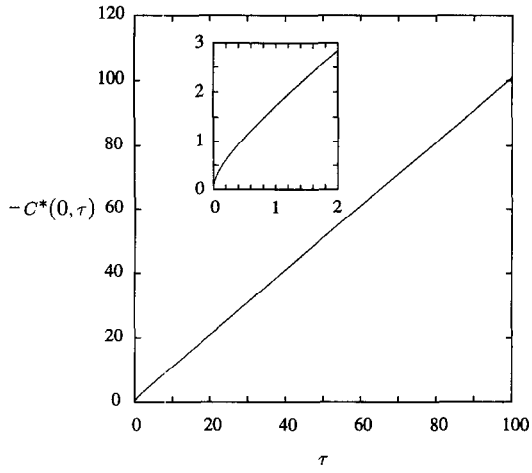

Fig. 3. Gas concentration at the solid–liquid interface ($\xi = 1$).

essentially the same as that given by equation (21). Based on this result, it is clear that bubble nucleation occurs at the solid–liquid interface at a certain time, no matter how small the initial gas concentration C_i (provided that it is larger than C_s, of course), since the gas concentration at the interface reaches the gas solubility limit in the liquid during the process. This greatly limits the thickness of the solid produced by any process at a constant solidification rate.

5. INTEGRAL SOLUTION AND RESULTS

Although there are situations where the solidification rate is constant (for example, unidirectional solidification), in most cases of interest the interface velocity varies with time. Exact analytic solutions are not always possible for every velocity function, therefore an approximate analytic solution is used in the present work. An integral method [11] is applied to solve equation (5) and the solution allows different functions for the solidification rate $V(t)$.

First, equation (5) is integrated over a dimensionless distance $\delta(\tau)$, called the concentration layer in order to remove from the differential equation the derivative with respect to the space dimensionless variable χ. The concentration layer is defined as the distance beyond which, for practical purposes, there is no gas diffusion. The initial gas concentration remains unaffected beyond $\delta(\tau)$. The resulting equation is

$$\frac{\partial}{\partial\tau}\left[\int_0^\delta C^*\,\mathrm{d}\chi\right] - C^*(\delta,\tau)\frac{\mathrm{d}\delta}{\mathrm{d}\tau} - \xi(\tau)[C^*]_0^\delta = \left[\frac{\partial C^*}{\partial\chi}\right]_0^\delta. \tag{22}$$

Using the boundary conditions, equations (7) and (8), leads to

$$\frac{\partial\gamma}{\partial\tau} = -\xi(\tau), \tag{23}$$

where

$$\gamma = \int_0^\delta C^*\,\mathrm{d}\chi. \tag{24}$$

A polynomial representation for $C^*(\chi,\tau)$ is assumed in the form

$$C^*(\chi,\tau) = \sum_{j=0}^{n} a_j(\tau)\chi^j, \tag{25}$$

with $n > 2$. In order to determine the $n+1$ coefficients a_j of the polynomial representation, $n+1$ conditions are needed. Two are given by the boundary conditions of the problem (equations 7 and 8). Other conditions may be obtained by differentiating equation (5) with respect to χ and applying it at $\chi = \delta$.

Substituting the polynomial profile into equation (24), the coefficients a_j can be determined as

$$a_0 = \frac{\xi\delta}{\xi\delta - n}, \tag{26}$$

$$a_j = \frac{(-1)^j\eta_j\xi\delta^{n-j}}{\xi\delta^n - n\delta^{n-1}},\ j \geqslant 1, \tag{27}$$

with

$$\eta_j = \begin{cases} n, & j = 1, \\ \displaystyle\sum_{j_1=1}^{n-j+1}\sum_{j_2=1}^{j_1}\cdots\sum_{j_{j-1}=1}^{j_{j-2}} j_{j-1}, & 2 \leqslant j \leqslant \mathrm{Int}(n/2), \\ n_{n-j}, & \mathrm{Int}(n/2) \leqslant j \leqslant n-1 \end{cases} \tag{28}$$

where $\mathrm{Int}(n/2)$ is the integer part of $n/2$, and

$$a_n = -\frac{\xi}{\xi\delta^n - n\delta^{n-1}}. \tag{29}$$

With the coefficients a_j determined, γ can be calculated as

$$\gamma = \sum_{j=0}^{n} a_j\frac{\delta^{j+1}}{j+1}. \tag{30}$$

Substituting γ in equation (23) and integrating with respect to τ, the gas diffusion integral equation gives

$$\delta = \frac{\sqrt{(n+1)^2\xi^2[I(\tau)]^2 + 4n(n+1)\xi I(\tau)} - (n+1)\xi I(\tau)}{2\xi}. \tag{31}$$

Note that the gas concentration at the interface is simply equal to a_0,

$$C^*(0,\tau) = a_0, \tag{32}$$

which is the maximum gas concentration in the liquid. Although making n very large does not necessarily guarantee a more accurate solution, it is interesting to

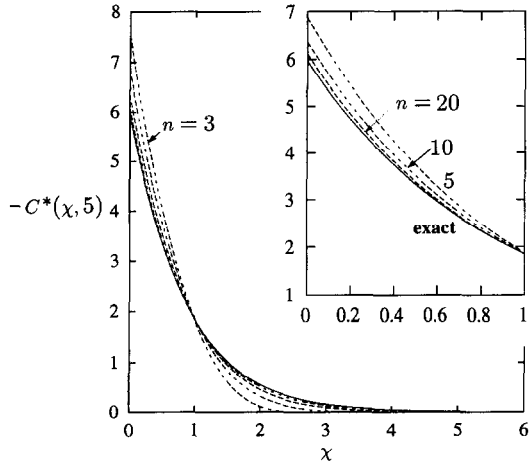

Fig. 4. Comparison between the approximate and the exact solutions for the concentration profiles ($\xi = 1$) for constant interface velocity and $\tau = 5$.

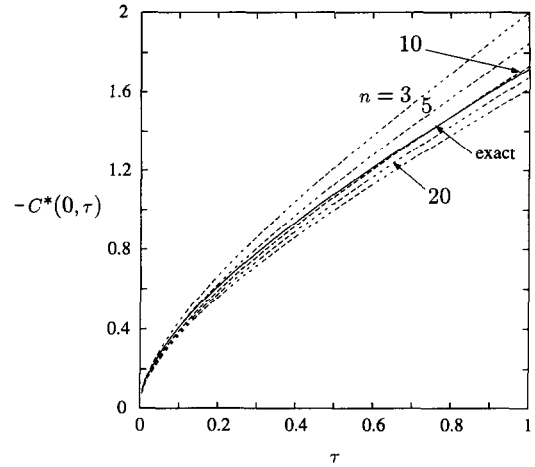

Fig. 6. Predictions of the gas concentration ($\xi = 1$) at the solid–liquid interface from both the exact and the integral method for small values of τ.

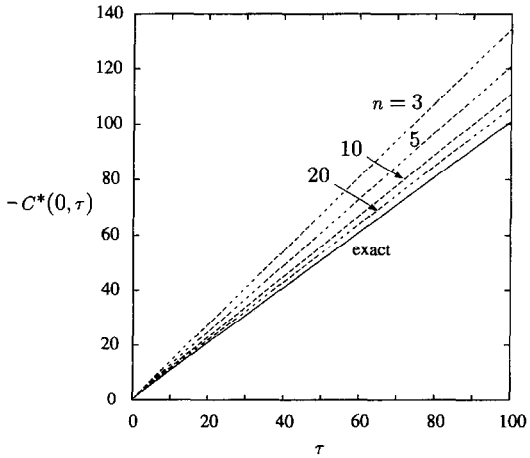

Fig. 5. Predictions of the gas concentration at the solid–liquid interface from both the exact and the integral method ($\xi = 1$).

note that the limit of a_0 when $n \to \infty$ exists and is given by

$$\lim_{n\to\infty} a_0 = 1 + \frac{2}{\sqrt{\xi^2[I(\tau)]^2 + 4\xi I(\tau)} - \xi I(\tau) - 2}. \tag{33}$$

5.1. *Constant solidification rate*

In order to validate the approximate solution, the integral method is used to obtain solutions for $\xi = 1$. Polynomial profiles defined by equation (25), with $n = 3$, 5, 10 and 20, were used to generate the results. Figure 4 shows the effect of n on the concentration profiles for $\tau = 5$. The profiles close to the interface are shown in the detail. Note that the higher the order of the polynomial approximation, the more accurate is the integral solution.

A comparison of the gas concentration at the interface based on the exact and approximate methods is illustrated in Fig. 5. It is clear that for large values of τ the interface concentration predicted by the integral solution is more accurate for larger values of n. For $n = 20$, the maximum relative error of the predicted interface concentration is 4.94% for $\tau > 0.5$.

As it can be seen in Fig. 6, the gas concentration at the interface predicted by the integral method behaves differently for small values of τ. The predictions based on the method are calculated for n of 3, 5, 10, 20 and ∞ [the last one using equation (33)]. It is interesting to note that for small values of τ the interface concentration calculated from the approximate solution can actually be smaller than the one based on the exact solution. This behavior could not be identified in Fig. 5 because of the range of values of τ. The departure from the exact solution indicates that greater values of n do not ensure a more accurate approximation. The maximum relative error for the integral solution for $n = 20$ is less than 10% for $\tau = 10^{-6}$.

It is worth noting that the integral solution overpredicts the dimensionless thickness of the gas species diffusion boundary layer. Equation (31) shows that the limit of δ when n tends to infinity is equal to infinity, while the scaling analysis previously discussed predicts $O(\delta)$ to be equal to 1 or $1/\tau$. The explanation for this fact is that even though the δ predicted from equation (31) increases indefinitely with n, the edge of the diffusion boundary layer is smaller than δ, i.e. the gas species concentrations calculated from the polynomial approximation for higher values of χ virtually vanish.

5.2. *Solidification rate inversely proportional to* $t^{1/2}$

For this case the analytical solution described in Section 4 is not applicable. The integral method is employed to predict the gas species concentration for $\xi = \tau^{-1/2}$. Figure 7 shows a comparison of the predicted gas concentrations at $\tau = 1$ for values of n of 3, 5, 10 and 20. It is clear that the concentrations predicted for larger n converge to a single curve.

The concentration profiles for τ of 0.1, 1, 5, 10 and

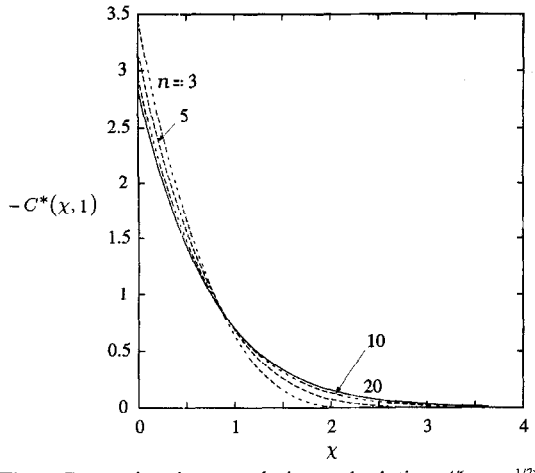

Fig. 7. Comparison between the integral solutions ($\xi = \tau^{-1/2}$) with values of n of 3, 5, 10 and 20 for $\tau = 1$.

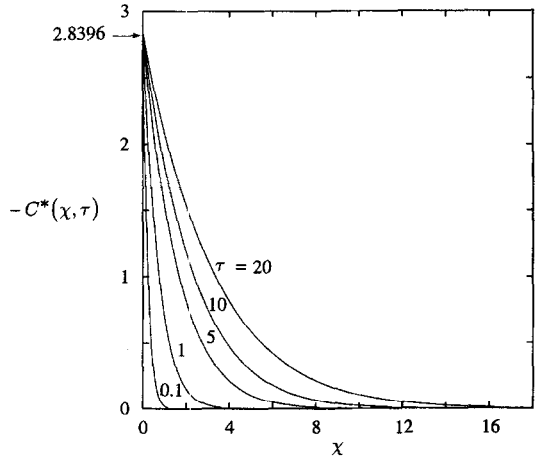

Fig. 8. Concentration profiles ($\xi = \tau^{-1/2}$) for τ of 0.1, 1, 5, 10 and 20, using the integral solution and $n = 20$.

20, for $n = 20$ are shown in Fig. 8. Note that the interface gas concentration is constant throughout the process and for $n = 20$, $C^*(0,\tau) = -2.8396$ ($\tau > 0$). It is also important to note that the gas boundary layer thickness increases gradually with time. The results are expected from the scale analysis for this case ($\xi = \tau^{-1/2}$). Both storage and diffusion have the same order of magnitude, and it is just a matter of substituting the interface velocity function to show that $\delta \sim \sqrt{\tau}$, for both cases when advection balances either diffusion or storage. This is due to the fact that both storage and diffusion have the same order of magnitude, and this can be easily concluded from the calculation of ε that leads to $\varepsilon \sim 1$. The interface gas concentration, in both cases, has the form $C^*(0,\tau) \sim -1$. This result supports the finding that the interface gas concentration is constant during the entire solidification process. At $\tau = 0$, $C^*(0,\tau)$ experiences an abrupt change from 0 to its constant value (-2.8396 for $n = 20$) and remains at this value for the rest of the phase change process.

The interface gas concentration $C^*(0,\tau)$ is equal to a_0 and the limit of a_0 when $n \to \infty$ could be calculated from equation (33), and it is found to be -2.7342. The relative error (relative to the value for $n \to \infty$) varies from 25.87% (for $n = 3$) to 3.85% (for $n = 20$). The relative errors presented here are intended only to illustrate the range of solutions found.

The implications of a constant gas concentration at the solid–liquid interface are drastic. Due to the fact that the absolute value of the dimensionless gas concentration is never higher than 2.8396 (for $n = 20$), it is easy to avoid the nucleation of gas bubbles at the solidification front. It is enough to have an initial gas concentration in the melt satisfying the following condition:

$$C_i < \frac{S - C^*(0,\tau)C_S}{1 - C^*(0,\tau)}, \tag{34}$$

where S is the gas solubility at the liquid phase. Therefore, if the initial gas concentration satisfies equation (34), there is no possibility of bubble nucleation.

6. EXPERIMENTAL VERIFICATION

Experimental verification of the results is obtained using a microscopic apparatus described by Bianchi and Viskanta [12]. Two controlled temperature reservoirs, which are heat exchangers made of copper and maintained at constant but different temperatures, are separated by a gap. The temperature of the hot reservoir is higher than the melting temperature of the sample and the temperature of the cold reservoir is lower. A stage made of aluminum is placed over the reservoirs and is moved at a constant velocity. Over the stage, the sample (air-saturated water) and a glass cover are located. Solidification of the sample occurs due to the controlled velocity from the hot reservoir in the direction of the cold reservoir. A reflection microscope is used to observe the solid–liquid interface of the sample. Reference is made to Bianchi and Viskanta [12] for details of the experimental apparatus and procedure.

Water saturated with air at 1 atmosphere is solidified at rates of 1, 10 and 100 μm s^{-1} and the nucleation of gas bubbles is photographed. The solid–liquid interface is shown in Fig. 9. For a solidification rate of 1 μm s^{-1} (Fig. 9(a)) almost no bubble nucleates (there are bubbles in some regions, but they do not appear in the region shown in the figure). For such a small solidification rate there is time for the segregated gas to diffuse back to the liquid, and the supersaturation is not sufficiently large for bubbles to nucleate at the entire solid–liquid interface. On the other hand, for a solidification rate of 10 μm s^{-1} (Fig. 9(b)), bubbles nucleate over the entire interface and are entrapped by the solid. For a higher solidification rate of 100 μm s^{-1} (Fig. 9(c)), bubble nucleation occurs in an even larger number of locations and the

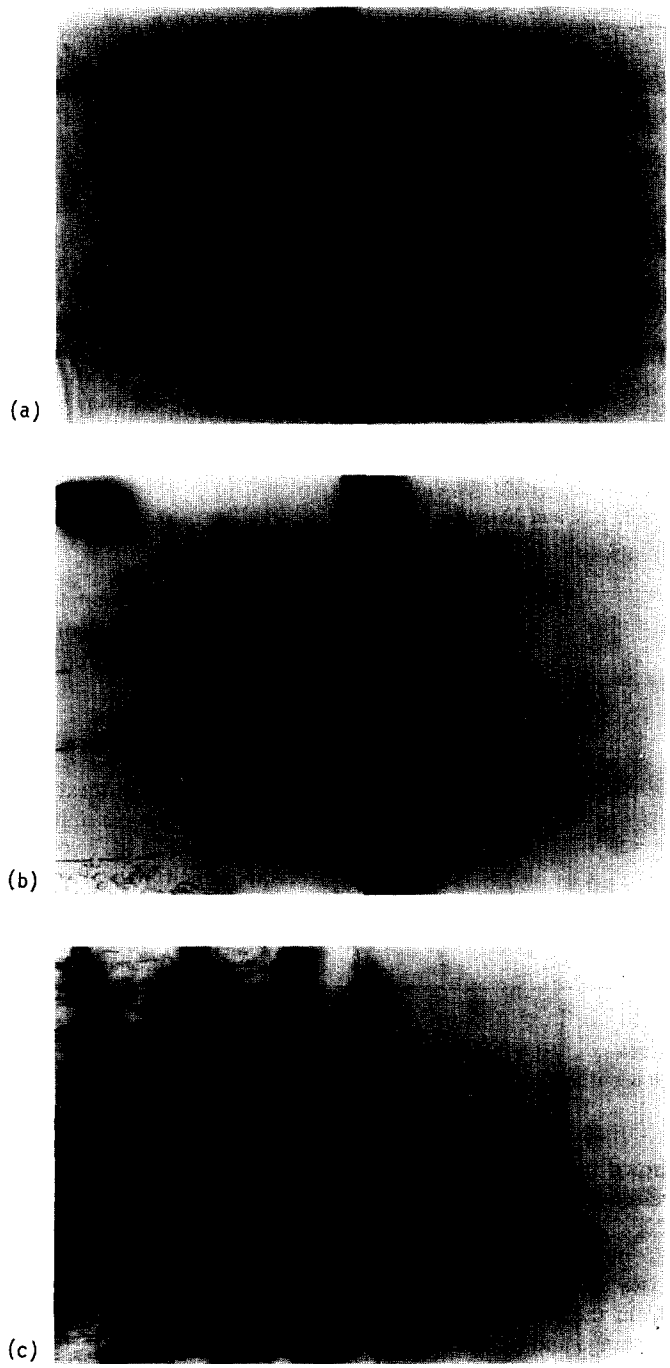

Fig. 9. Bubble nucleation during the solidification of air saturated water for three different solidification rates: (a) $V = 1\ \mu m\ s^{-1}$; (b) $V = 10\ \mu m\ s^{-1}$; (c) $V = 100\ \mu m\ s^{-1}$.

resulting bubbles in the solid are smaller because there is no time for them to grow prior to the freezing of the surrounding liquid. It is evident that the gas concentration at the solid–liquid interface is larger for a higher solidification rate as predicted by the results using the analytical and integral solution methods.

It should be noted that this experimental verification is only qualitative. Prior to establishing a stagnant solid–liquid interface, transient motion occurs due to undercooling of the melt. The initial gas concentration in the liquid is not uniform, because the needed undercooling to freeze the water segregates gas at the solidification front. Therefore, the experiment performed does not truly mimic the analysis presented.

7. CONCLUDING REMARKS

The problem of gas evolution during solidification has been investigated. An exact solution was found

for the case when the interface velocity is constant. An integral method was employed to obtain an approximate analytical solution to the problem for any solidification rate function. In particular, a solidification rate inversely proportional to the square root of time was used because the vast majority of solidification processes, even including buoyancy effects, present this form of the interface velocity. A scale analysis was used to predict the order of magnitude of the different parameters for the process and the results were found to be consistent with the solutions obtained using both the analytical and the integral methods. Qualitative experimental validation was obtained by observing the rate of bubble nucleation for three different solidification rates.

The results obtained for the integral method for a constant solidification rate show an excellent agreement with the exact analytical solution for the case of constant solid–liquid interface velocity. The relative error is smaller than 5% for $n = 20$ ($\tau \geqslant 0.5$). For a constant solidification rate the maximum gas concentration of the liquid increases with time and has no upper limit. Therefore, gas bubbles will nucleate at some time during solidification and there is a maximum solid layer thickness that can be formed during the phase change process before nucleation occurs. This is a major limitation of using a constant solidification rate to produce solids from melts that dissolve a large amount of gas.

The integral method predicts a constant interface gas concentration for solidification rates inversely proportional to the square root of time. Therefore, it is easy to avoid the nucleation of gas bubbles during the solidification process, because the only condition to be satisfied is that stated by equation (34). Since the integral method may be applied for any interface velocity function of time, results can be readily obtained without the need of significant computational efforts.

To establish confidence in the numerical results, the model predictions should be validated by comparing with quantitative experimental data. Due to the fact that the gas diffusion boundary layer thickness is extremely small, it is very challenging to design and build an experimental apparatus to measure the gas concentration ahead of the solidification front.

Acknowledgment—Marcus V. A. Bianchi gratefully acknowledges support by the Conselho Nacional de Desenvolvimento Científico e Technológico (CNPq, Brazil).

REFERENCES

1. Kurz, W. and Fisher, D. J., *Fundamentals of Solidification*, 3rd edn. Trans Tech Publications, Aedermannsdorf, Switzerland, 1989, Chapter 1.
2. Colangelo, V. J. and Heiser, F. A., *Analysis of Metallurgical Failures*, 2nd edn. John Wiley, New York, 1987, Chapter 11.
3. Eastwood, L. W., *Gas in Light Alloys*. John Wiley, New York, 1946, Chapter 1.
4. Wilcox, W. R. and Kuo, V. H. S., Gas bubble nucleation during crystallization. *Journal of Crystal Growth*, 1973, **19**, 221–228.
5. Vasconcellos, K. F. and Beech, J., The development of blowholes in the ice/water/carbon dioxide system. *Journal of Crystal Growth*, 1975, **28**, 85–92.
6. Boomgaard, J. V. D., Gas bubble formation ahead of a solidification front. *Phillips Journal of Research*, 1978, **33**, 149–185.
7. Tagavi, K., Chow, L. C. and Solaiappan, O., Void formation in unidirectional solidification. *Experimental Heat Transfer*, 1990, **3**, 239–255.
8. Sulfredge, C. D., Chow, L. C. and Tagavi, K. A., Solidification void formation for cylindrical geometries. *Experimental Heat Transfer*, 1990, **3**, 257–268.
9. Poirier, D. R. and Geiger, G. H., *Transport Phenomena in Materials Processing*. TMS, Warrendale, PA, 1994, Chapter 10.
10. Bejan, A., *Convection Heat Transfer*. John Wiley, New York, 1984, p. 17.
11. Özişik, M. N., *Heat Conduction*, 2nd edn. Wiley Interscience, New York, 1993, Chap. 6.
12. Bianchi, M. V. A. and Viskanta, R., On the morphology of ice crystals grown from ammonium chloride solutions. In *Transport Phenomena in Solidification*, ed. C. Beckermann, H. P. Wang, L. A. Bertram, M. S. Sohal and S. I. Güçeri. ASME, New York, 1994.